



Probing the Structure of SDSS J1004+4112 through Microlensing Analysis of Spectroscopic Data

C. Fian¹, J. A. Muñoz^{1,2}, R. Forés-Toribio^{1,2}, E. Mediavilla^{3,4},
J. Jiménez-Vicente^{5,6}, D. Chelouche^{7,8}, S. Kaspi⁹ and
G. T. Richards¹⁰

¹Departamento de Astronomía y Astrofísica, Universidad de Valencia, E-46100 Burjassot, Valencia, Spain. email: carina.fian@uv.es

²Observatorio Astronómico, Universidad de Valencia, E-46980 Paterna, Valencia, Spain

³Instituto de Astrofísica de Canarias, Vía Láctea S/N, La Laguna 38200, Tenerife, Spain

⁴Departamento de Astrofísica, Universidad de la Laguna, La Laguna 38200, Tenerife

⁵Departamento de Física Teórica y del Cosmos, Universidad de Granada, Campus de Fuentenueva, 18071 Granada, Spain

⁶Instituto Carlos I de Física Teórica y Computacional, Universidad de Granada, 18071 Granada, Spain

⁷Department of Physics, Faculty of Natural Sciences, University of Haifa, Haifa 3498838, Israel

⁸Haifa Research Center for Theoretical Physics and Astrophysics, University of Haifa, Haifa 3498838, Israel

⁹School of Physics and Astronomy and Wise Observatory, Raymond and Beverly Sackler Faculty of Exact Sciences, Tel-Aviv University, Tel-Aviv 6997801, Israel

¹⁰Department of Physics, Drexel University, 32 S. 32nd Street, Philadelphia, PA 19104, USA

Abstract. We aim to uncover the structure of the continuum and broad emission line (BEL) emitting regions in the gravitationally lensed quasar SDSS J1004+4112 through unique microlensing signatures. Analyzing 20 spectroscopic observations from 2003 to 2018, we study the striking deformations of various BEL profiles and determine the sizes of their respective emitting regions. We use the emission line cores as a baseline for no microlensing and then apply Bayesian methods to derive the sizes of the Ly α , Si IV, C IV, C III], and Mg II emitting regions, as well as of the underlying continuum-emitting sources. We find that the sizes of the emitting regions for the BELs are a few light-days across, notably smaller than in typical lensed quasars. The asymmetric distortions observed in the BELs suggest that the broad-line region lacks spherical symmetry and is likely confined to a plane. The inferred continuum emitting region sizes are larger than predictions based on standard thin-disk theory by a factor of ~ 4 . We find that the size-wavelength relation is in agreement with that of a geometrically thin and optically thick accretion disk.

Keywords. gravitational lensing: strong – gravitational lensing: micro – quasars: general – quasars: emission lines – quasars: individual (SDSS J1004+4112)

1. Introduction

SDSS J1004+4112 is the first quasar known to be lensed by a foreground cluster of galaxies and was discovered in the Sloan Digital Sky Survey (Inada et al. 2003). The lensed quasar comprises four bright images at a source redshift of $z_s = 1.73$. These images are produced by a massive cluster at a lens redshift of $z_l = 0.68$, and the maximum separation angle is $14''.6$ between components B and C. The system has been monitored photometrically (Fohlmeister et al. 2007, 2008; Fian et al. 2016; Muñoz et al. 2022), and the time-delays for three of the quasar images (A, B, and C) were measured by Fohlmeister et al. (2007, 2008). A recent study by Muñoz et al. (2022) found a time delay of 2458.47 ± 1.02 days between the trailing image D and the leading image C, which is the longest delay ever measured for a gravitationally lensed quasar.

Optical microlensing, induced by stars in the cluster halo or nearby satellites, is a recognized phenomenon in the lens system SDSS J1004+4112. This effect has been used to estimate the size of the continuum-emitting source in the lensed quasar (Fohlmeister et al. 2008; Fian et al. 2016). Alongside the differential brightness variation of the images in photometric passbands, microlensing effects have also been identified in the spectral lines (Richards et al. 2004; Lamer et al. 2006; Gómez-Álvarez et al. 2006; Motta et al. 2012; Popović et al. 2020; Fian et al. 2018, 2021). Spectroscopic analyses of the individual components have unveiled significant differences in the emission line profiles. Particularly, component A displays an enhanced blue wing in various high-ionization lines relative to the other components, which has been interpreted as an indication of microlensing in image A. Recent research by Hutsemékers et al. (2023) has demonstrated that the distortion of the C IV emission line profile in SDSS J1004+4112 can be explained using simple broad-line region (BLR) models. Our study expands upon this by extensively analyzing existing spectroscopic data, including additional observational epochs and a wider range of spectral lines compared to Hutsemékers et al. (2023). Moreover, we undertake a comprehensive global analysis encompassing line cores, line wings, and the adjacent continuum, deepening our insight into the diverse light-emitting regions within the quasar.

2. Observations and Data Analysis

We have assembled a set of rest-frame UV spectra for the images A, B, C, and D of the gravitationally lensed quasar SDSS J1004+4112. Our dataset consists of 20 published spectra, spanning a 15-year period from February 2003 to February 2018. These spectra cover a range of typical high- and low-ionization lines found in quasars, including Ly α , Si IV, C IV, C III], and Mg II. In Figure 1, we show the average of these line profiles for each lensed image observed in at least two different epochs. We also include one, two, and three-sigma intervals to highlight the variability in the line wings and other emission species. We observe significant variability in the blue wings of Si IV, C IV, and C III] in image A, as well as in the red wing of Ly α and the shelf-like feature at $\sim \lambda 1610$ (blueward of He II).

Emission line cores arise from large, spatially extended regions that are not significantly affected by microlensing and intrinsic variability (Guerras et al. 2013; Fian et al. 2018). Measuring core flux ratios between lensed images provides a robust method for establishing a microlensing-free reference point. To remove the continuum from each image and emission line, we apply a linear fit to both sides of the emission line's continuum and subtract it from the spectrum. The core fluxes are then defined by a narrow interval centered on the peak of the line. Our inferred core flux ratios align well with infrared flux ratios reported by Ross et al. (2009) and show consistency with radio flux ratios observed by Jackson (2020), Hartley et al. (2021), and McKean et al.

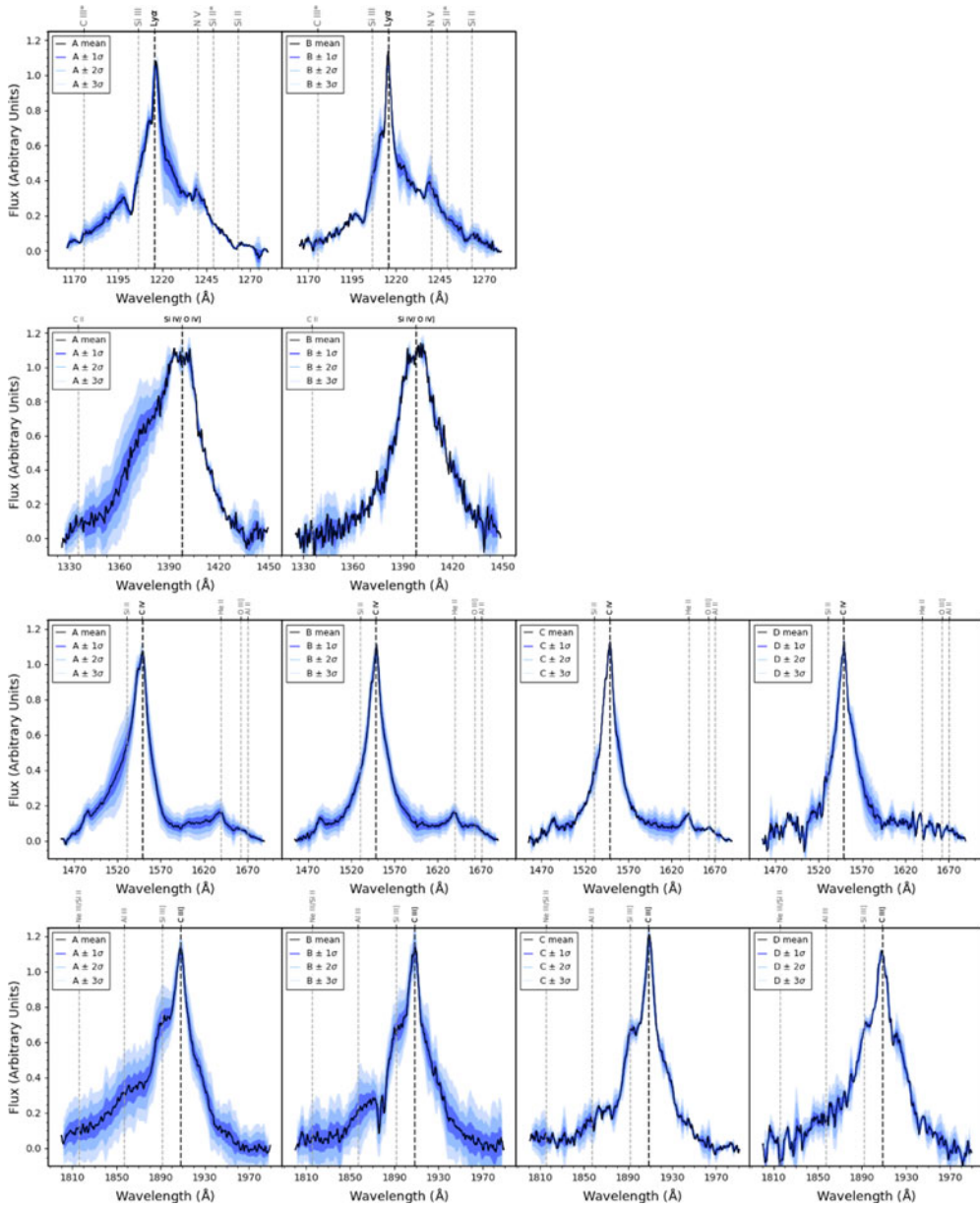


Figure 1. Average (black) spectra of the Ly α , Si IV, C IV, and C III] emission lines (from top to bottom). The one, two, and three sigma intervals for the images A, B, C, and D (left to right) are depicted in dark blue, blue, and light blue, respectively.

(2021). Microlensing, which is sensitive to the source size (where smaller regions experience higher magnifications), offers valuable insights into the structure and kinematics of quasar accretion disks. Quantifying the microlensing impact on the continuum requires disentangling it from macro-lensing magnification effects (stemming from the smooth lensing potential) and extinction. We correct for these effects by assessing the differences between the continuum adjacent to emission lines, $(m_x - m_B)_{cont}$, and the magnitude differences of emission line cores, $(m_x - m_B)_{core}$, between the images x (where $x = A, C, D$) relative to image B, $\Delta\mu_{cont} = (m_x - m_B)_{cont} - (m_x - m_B)_{core}$. Image B

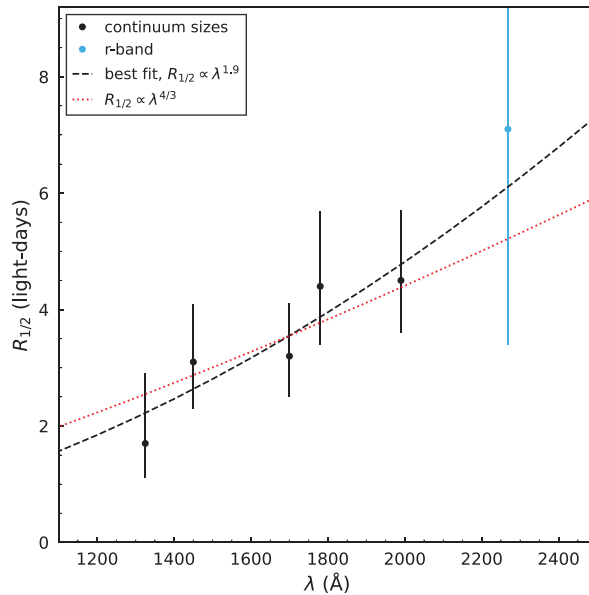


Figure 2. Continuum-emitting region sizes derived from microlensing, plotted against wavelength. The dashed black line shows the best fit to the data ($\beta \sim 1.9$). The red dotted line represents a fit with a fixed theoretical power-law index of $\beta = 4/3$.

is chosen as the reference as it is less affected by microlensing variability compared to image A (Hutsemékers et al. 2023). Additionally, it benefits from a more extensive set of observational epochs compared to images C and D. To determine the sizes of BEL-emitting regions, we normalize the continuum-subtracted spectra for all images and epochs to match the emission line core. We then assess the microlensing in the line wings ($\Delta\mu_{wing} = (m_x - m_B)_{wing} - (m_x - m_B)_{core}$) on either side of the emission line peak, corresponding to a velocity range of 3000 – 10000 km s⁻¹.

3. Methods and Results

Given the observed differential microlensing in the wings and adjacent continua of various emission lines between lensed images, we can deduce the size of their emission regions. We employed a statistical approach, treating each microlensing measurement as a single epoch. All available epochs were used to calculate the joint microlensing probability to derive an average size estimate, as detailed in Guerras et al. (2013) and Fian et al. (2018, 2021). Inferring differential microlensing from the spectroscopic data of lensed quasars is complex due to time-delayed intrinsic flux variations between images. Deformations in the BELs caused by intrinsic variability can resemble microlensing, leading to potential inaccuracies in source size measurements. For the lensed quasar SDSS J1004+4112, this issue is particularly pronounced for images C and D, which have long time delays (~ 6.7 years) relative to other images in the system. To ensure accurate interpretation, our focus will be on the magnitude differences between images A and B, given their short time lag (~ 44 days), as these differences can most likely be attributed to microlensing.

Figure 2 illustrates the microlensing-based continuum sizes as a function of wavelength. To fit our size spectrum, we utilized the power-law index β — representing the disk’s temperature profile — as an adjustable parameter, achieving the most optimal fit at $\beta \sim 1.9$. The inferred sizes and the physical model are consistent with the slope expected for an optically thick and geometrically thin accretion disk model ($\beta = 4/3$). While numerous microlensing studies have found sizes significantly larger than predicted

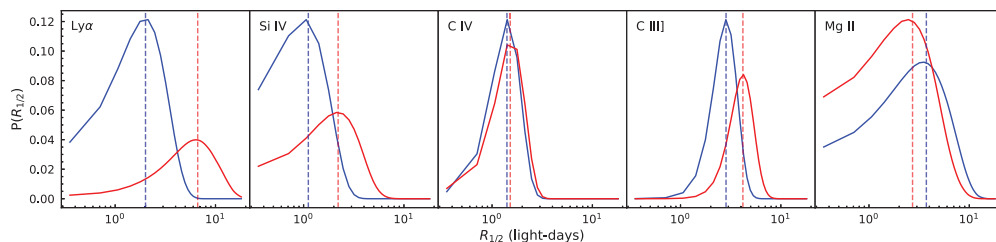


Figure 3. Probability density functions of the half-light radius $R_{1/2}$ for the blue and red wings of Ly α , Si IV, C IV, C III], and Mg II (left to right). The vertical dashed lines denote the expected emission region size.

by existing accretion disk theories, corroborating our results (~ 4 larger than theoretical predictions), they often report flatter size-wavelength relationships (Blackburne *et al.* 2011; Jiménez-Vicente *et al.* 2014). To affirm the accuracy of our results, we compared the r-band continuum size derived from our spectroscopic data with that acquired from 14.5 years of photometric monitoring data (Muñoz *et al.* 2022). The outcomes from the two distinct datasets align well, with $R_{1/2} = 7.1^{+7.4}_{-3.7}$ lt-days for the spectroscopic data, and $R_{1/2} = 5.3^{+1.3}_{-0.7}$ lt-days for the photometric observations (Forés-Toribio *et al.* submitted). In Figure 3, we display the probability density functions for the regions emitting the broad wings of Ly α , Si IV, C IV, C III], and Mg II. Intriguingly, we find that the sizes of the regions emitting the BELs are often very small, occasionally even smaller than the sizes associated with the optical continuum-emitting region. These results differ significantly (by an order of magnitude) from the BLR size estimates reported in Guerras *et al.* (2013), and they also contrast with the average BLR sizes determined for a sample of lensed quasars in prior studies (Fian *et al.* 2018, 2021). However, our inferred half-light radius for the C IV BLR is in agreement with the recent measurement by Hutsemékers *et al.* (2023) ($R_{1/2} = 2.8^{+2.0}_{-1.7}$ lt-days), lending credence to the reliability of our findings.

4. Conclusions

SDSS J1004+4112 stands out as an extensively studied lensed quasar, with abundant photometric monitoring data and spectroscopic observations available. Although recognized early as a lensed quasar with BEL deformation, understanding the line distortions and inter-component differences remained incomplete. With 20 spectroscopic observations, we thoroughly analyzed the Ly α , Si IV, C IV, C III], and Mg II lines, plus adjacent continua, and we constrained their emitting region sizes. We unveiled agreement in the line core ratios between the lensed quasar images, serving as a microlensing-free reference, and mid-IR/radio ratios reported in the literature (Ross *et al.* 2009; Jackson 2020; Hartley *et al.* 2021; McKean *et al.* 2021). The inferred sizes of the continuum-emitting regions increase with wavelength, supporting the idea of disk reprocessing, and are larger by a factor of ~ 4 than predicted by a standard thin disk. This discrepancy is consistent with recent studies (Jiménez-Vicente *et al.* 2014; Fian *et al.* 2023), possibly resulting from a significant contribution of diffuse BLR emission to the observed continuum signals (see, e.g., Chelouche *et al.* 2019; Korista & Goad 2019; Netzer 2022; Fian *et al.* 2023). Notably, our spectroscopic r-band continuum size ($R_{1/2} = 7.1^{+7.4}_{-3.7}$ lt-days) matches well with the photometric data-based size ($5.3^{+1.3}_{-0.7}$ lt-days; see also Forés-Toribio *et al.* submitted). Using Bayesian analysis, we determined the emission region sizes for Ly α , Si IV, C IV, C III], and Mg II. Our findings show that these regions are a few light-days across, significantly smaller than average quasar BLRs (usually tens of light-days; Guerras *et al.* 2013; Fian *et al.* 2018, 2021). Intriguingly, some BEL-emitting region sizes are smaller

than the optical continuum. A plausible interpretation for this surprising outcome could be that the BEL-emitting regions are located close to a caustic, while the accretion disk is farther away from it. Should the BLR, or a part thereof, be situated on or near a caustic while the accretion disk is located farther from it, the BLR would experience substantial magnification, whereas the accretion disk would undergo less magnification. While this situation is expected to be uncommon, it could conceivably account for the microlensing anomalies observed in this lensed system.

References

- Blackburne, J. A., Pooley, D., Rappaport, S., et al. 2011, *ApJ*, 729, 34.
Chelouche, D., Pozo Nuñez, F., & Kaspi, S. 2019, *Nature Astronomy*, 3, 251.
Fian, C., Mediavilla, E., Hanslmeier, A., et al. 2016, *ApJ*, 830, 149.
Fian, C., Guerras, E., Mediavilla, E., et al. 2018, *ApJ*, 859, 50.
Fian, C., Mediavilla, E., Motta, V., et al. 2021, *A&A*, 653, A109.
Fian, C., Chelouche, D., & Kaspi, S. 2023, arXiv:2307.14824.
Fohlmeister, J., Kochanek, C. S., Falco, E. E., et al. 2007, *ApJ*, 662, 62.
Fohlmeister, J., Kochanek, C. S., Falco, E. E., et al. 2008, *ApJ*, 676, 761.
Gómez-Álvarez, P., Mediavilla, E., Muñoz, J. A., et al. 2006, *ApJ*, 645, L5.
Guerras, E., Mediavilla, E., Jimenez-Vicente, J., et al. 2013, *ApJ*, 764, 160.
Hartley, P., Jackson, N., Badole, S., et al. 2021, *MNRAS*, 508, 4625.
Hutsemékers, D., Sluse, D., Savić, D., et al. 2023, *A&A*, 672, A45.
Inada, N., Oguri, M., Pindor, B., et al. 2003, *Nature*, 426, 810.
Jackson, N. 2020, *ApJ*, 900, L15.
Jiménez-Vicente, J., Mediavilla, E., Kochanek, C. S., et al. 2014, *ApJ*, 783, 47.
Korista, K. T. & Goad, M. R. 2019, *MNRAS*, 489, 5284.
Lamer, G., Schwobe, A., Wisotzki, L., et al. 2006, *A&A*, 454, 493.
McKean, J. P., Luichies, R., Drabent, A., et al. 2021, *MNRAS*, 505, L36.
Motta, V., Mediavilla, E., Falco, E., et al. 2012, *ApJ*, 755, 82.
Muñoz, J. A., Kochanek, C. S., Fohlmeister, J., et al. 2022, *ApJ*, 937, 34.
Netzer, H. 2022, *MNRAS*, 509, 2637.
Popović, L. Č., Afanasiev, V. L., Moiseev, A., et al. 2020, *A&A*, 634, A27.
Richards, G. T., Keeton, C. R., Pindor, B., et al. 2004, *ApJ*, 610, 679.
Ross, N. R., Assef, R. J., Kochanek, C. S., et al. 2009, *ApJ*, 702, 472.